www.elsevier.com/locate/memsci

Vacuum-Assisted Tailoring of Pore Structures of Phenolic Resin Derived Carbon Membranes

Siti Nurehan Abd Jalil, David K. Wang, Christelle Yacou, Julius Motuzas, Simon Smart, João C. Diniz da Costa

PII: S0376-7388(16)31702-1
DOI: http://dx.doi.org/10.1016/j.memsci.2016.11.002
Reference: MEMSCI14838

To appear in: *Journal of Membrane Science*

Received date: 20 September 2016
Revised date: 1 November 2016
Accepted date: 3 November 2016

Cite this article as: Siti Nurehan Abd Jalil, David K. Wang, Christelle Yacou, Julius Motuzas, Simon Smart and João C. Diniz da Costa, Vacuum-Assisted Tailoring of Pore Structures of Phenolic Resin Derived Carbon Membranes *Journal of Membrane Science,* http://dx.doi.org/10.1016/j.memsci.2016.11.002

Vacuum-Assisted Tailoring of Pore Structures of Phenolic Resin Derived Carbon Membranes

Siti Nurehan Abd Jalil[1,2], David K. Wang[1], Christelle Yacou[1,3], Julius Motuzas[1], Simon Smart[1], João C. Diniz da Costa[1]*

[1]The University of Queensland, FIM²Lab – Functional Interfacial Materials and Membranes Laboratory, School of Chemical Engineering, Brisbane, Qld 4072, Australia.

[2]Universiti Teknologi MARA (UiTM), Faculty of Chemical Engineering, 40450 Shah Alam, Selangor, Malaysia.

[3]Université des Antilles, Department of Engineering, BP 250, 97157 Pointe à Pitre Cedex, Guadeloupe, France.

Abstract

This work shows the preparation and separation performance assessment of carbon membranes derived from phenolic resin by a vacuum-assisted method and carbonisation in an inert atmosphere. The vacuum time played an important role in tailoring the structure of the membranes. For instance, pore volumes and surface areas increased from 0.81 and 834 to 2.2 cm^3 g^{-1} and 1910 m^2 g^{-1}, respectively, as the vacuum time exposure increased from 0 to 1200 s. The significant structural changes correlated very well with water permeation, as fluxes increased by 91% as the vacuum time increased from 0 to 1200s, reaching up to 169 kg m^{-2} h^{-1} at 5 bar. Molecular weight cut-off tests showed no rejection for the smaller glucose and sucrose molecules, though this increased to ~ 80% and full rejection for 36kD and 400kD polyvinyl pyrrolidine. Interestingly, FTIR spectra showed that the peaks of C-H stretching vibration (2800-3200 cm^{-1}) and C-O stretching (1030 cm^{-1}) became more pronounced as a function of increasing vacuum time, strongly suggesting that the use of vacuum further assisted in the polycondensation of phenolic oligomers. Based on these outcomes, a cluster to cluster model is proposed, whereby vacuum application promoted crosslinking reactions of the phenolic resin, creating microporous regions within the clusters, and mesoporous regions between the clusters.

Graphical Abstract

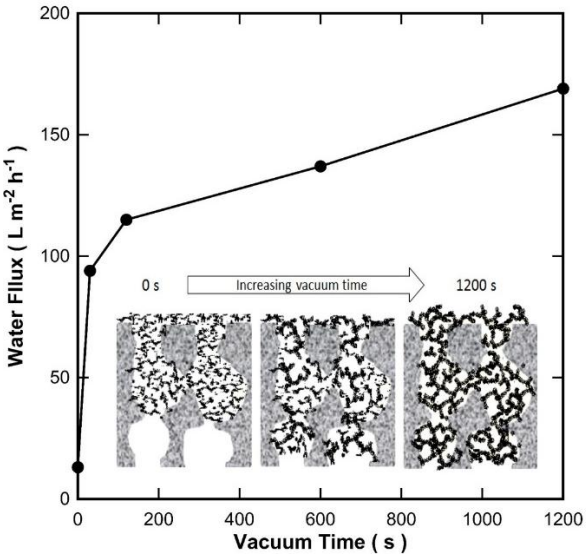

Keywords: carbon membranes; vacuum-assisted method; water; molecular weight cut-off.

1. Introduction

Inorganic membranes have a wide range of industrial applications for processing liquids and coupled with the large number of available inorganic materials, makes this field of research attractive to solve separation problems. Applications such as alumina membranes for juice processing [1], protein separation [2], and oil/water emulsion separation [3], titania membranes for wastewater processing [4], zirconia membranes for processing vegetable oil [5] and food [6], zeolites for the dehydration of organic solvents [7], cobalt silica membranes for ammonia separation from waste waters [8] and carbonized templated silica membranes for desalination [9] are some of many examples. Inorganic membranes have a very wide range of pore sizes from microfiltration to

ultrafiltration to nanofiltration and even down to the sub-nanometer range depending on the materials of choice and synthesis conditions.

One material of interest in this field is carbon derived membranes following the pioneering work of Koresh and Soffer [10] in 1983, who initiated extensive research activity in micropore tailoring of carbon by pyrolysing polyimide hollow fibres, where pore sizes are typically in the region of 3-6Å [11]. Subsequently, a variety of precursor materials were used to prepare carbon membranes, including derivatives of polyimides [12, 13], polyfurfuryl alcohol (PFFA) [14], phenolic resins [15-18], polyacylonitrile [19], and polymers of intrinsic microporosity (PIM) [20]. Carbon membranes have been extensively developed for gas separation, though also investigated for liquid separation including oil/water [21], desalination [22], de-colorization of coke furnace wastewater [23], pervaporation of azeotropic benzene–cyclohexane mixtures [24], oil and water separation [25] and separation of chromium (VI) in ultrafiltration of water solutions [26] as representative examples. An advantage of carbon membranes is related to the good stability conferred by carbon structures.

The pore dimension of carbon membranes can be finely adjusted by thermo-chemical treatment (pyrolysis or carbonization) to give narrow pore size distributions [27] and temperature plays an important role in the microporosity formation [28, 29]. Lately, polymeric precursors have been coated on the surface of porous ceramic substrates followed by carbonization in an inert atmosphere up to 800 °C, or even higher depending on the desired structural features of the carbon membrane matrix. Ceramic substrates have been reported to provide ideal surfaces for the coating of phenolic resins, particularly porous alumina tubes which allow this technology to be scaled up. This has been shown by Pacheco Tanaka and co-workers [30-33] by coating novolac and resol phenolic resins, or by mixing alpha-alumina with novolac. A very recent development involves the preparation of carbon-alumina mixed matrix membranes, where the phenolic resin was incorporated into the porous structure of an alumina substrate by a vacuum impregnation, showing that the vacuum time played an important role in the structural formation of the mixed matrix membranes [22]. Phenolic resins have several advantages for the preparation of CMS membranes such as better control of its crosslinking density, molecular weight and pore size by sol-gel chemistry and carbonization process [34-37]. Other types of polymers as carbon precursors, like polyimide, can also produce high quality CM membranes. However, polymers have very large poly-dispersity and molecular weight distribution, the degree of manipulation of material property is restricted, contrary to phenolic resins.

In this work we report the effect of a vacuum-assisted method as a pre-treatment of carbon thin films using a phenolic resin, prior to curing and carbonization. Contrary to the carbon-alumina mixed matrix membranes, the carbon membranes in this work were formed by dip-coating a phenolic resin solution on an alumina substrate, thus forming a resin thin film first. The membranes were subsequently exposed to a desired vacuum time, followed by curing and carbonization in an inert nitrogen atmosphere, resulting in a carbon thin film. Carbon materials were also prepared in the same fashion as the membranes and characterized using TGA, FTIR and nitrogen adsorption. The characterization work was correlated to the performance of the carbon membranes, and a mechanism is proposed to explain the structural tailoring of the porous carbon matrix.

2. Experimental

2.1 Materials and characterisation

Phenolic resin Resinox IV-1058 (see chemical structure in the appendix Fig. A1) was used as precursor to prepare carbon materials and membranes (CM). The resin was mixed with methanol at 1:10 wt% ratio and aged under stirring for 2 hours at room temperature. Subsequently, a small amount of the resultant solution was dispensed in a petri dish to form a thin resin film. The petri dish was directly placed inside a closed desiccator where a vacuum was applied for a desired period. Then the samples were cured in an oven at 60 °C for 24 hours. These samples are abbreviated as resin gel (RG) followed by a number which indicates the vacuum time. For instance, RG600 is a resin gel sample exposed to 600 s of vacuum time. The RG samples were placed in a furnace with a PID temperature controller and carbonised in an inert nitrogen atmosphere with a ramping and cooling rate of 5 °C min^{-1} up to 700 °C and a dwell time of 2.5 h.

Structural properties of the CM material were analysed using an ASAP 2020 apparatus (Micromeritics Instrument Corporation). The samples were degassed at 200 °C for 24 hours under high vacuum prior to nitrogen adsorption at 77 K. Specific surface areas and pore volume were calculated via the multi-point Brunauer-Emmett-Teller (BET) model and the pore size distribution was determined using a Barrett-Joyner-Halenda (BJH) model. Thermogravimetric analysis (TGA) of the RG samples was carried out using a differential scanning calorimeter / thermogravimetric analyser (Mettler-Toledo, TGA/DSC 1) from 30 to 1000 °C at the same carbonisation conditions as the CM materials. The RG and CM materials were also characterized by using a Shimadzu IRAffinity-1 Fourier-transform infrared spectrometer with a Pike MIRacle attenuated total

reflectance accessory (ATR-FTIR) to determine the functional groups of the precursor phenolic resin after curing (RG samples) and after carbonisation (CM samples).

2.2 Membrane preparation, characterisation and testing

All CM membranes were coated on the outer shell of alumina tubular substrates (Ceramic Oxide Fabricators, Melbourne, Australia), with details of the substrate listed in Table 1. A dip coating method was used, where a substrate was immersed into the phenolic resin solution for 1 min of holding time with 10 cm min^{-1} dipping and withdrawal rate. After dip coating, the membrane was immediately exposed to a vacuum pressure (< 1 Torr) via the inner shell of the tube for a desired time (from 30 to 1200 s). Subsequently, the coated membranes were cured and carbonised in the same manner as the CM materials described above. The CM nomenclature is also used, where CM30 membrane refers to carbonised membranes exposed to vacuum for a period of 30 s. The cross section and surface of the resultant CM membranes were analysed by scanning electron microscope (SEM, JEOL JSM-7001F) with a hot (Schottky) electron gun at an accelerating voltage of 10 kV.

.

Table 1. The properties of porous alumina substrate

Material	α-Al_2O_3
Mean pore diameter (nm)	100
Dimensions (mm)	Outer diameter: 10 ; inner diameter: 7
Length (cm)	4.3-5.3
Pre-treatment	Calcined in air at 1000 °C for 8 hours

The CM membranes were tested for permeation and the rejection of organic substances using a permeation rig as schematically shown in Fig. 1. A pressure vessel was used to hold an aqueous solution of interest which was pressurised to a desired pressure (valve V-1) using nitrogen gas from a high pressure cylinder. This provided the driving force (i.e. pressure gradient) for the permeation of water through the membrane which was placed in a membrane module. Permeation testing was carried out in a dead-end mode, where the retentate stream was closed. The permeate stream was collected in a beaker on an electronic scale linked to a computer.

The flux, J_v (L m^{-2} h^{-1}) was calculated using the follow equation:

$$J_v = \frac{\Delta W}{A\Delta t} \quad (1)$$

where ΔW is the permeated mass (kg) collected over a predetermined time Δt (h) at steady state, and A is the effective permeation area (m^2). The collected permeate was analysed using a Shimadzu UV-2700 UV-Vis spectrometer to determine the concentration of organic substances (i.e. glucose, sucrose, polyvinyl pyrrolidine (PVP molecular weights of 36kD and 400kD) against calibrated curves. The rejection (R) of substances was calculated using the following equation:

$$R(\%) = \left[1 - \left(\frac{C_p}{C_f}\right)\right] \times 100 \quad (2)$$

where C_p and C_f are the concentrations of the solute in the permeate and feed streams, respectively.

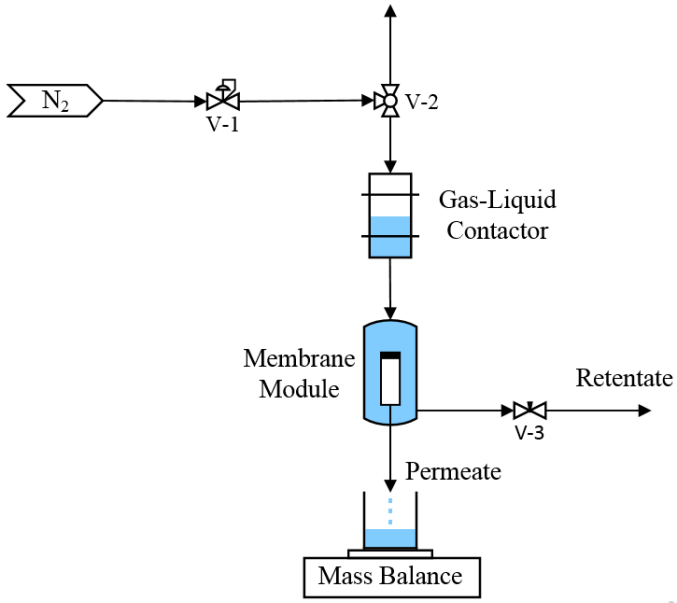

Fig. 1. Schematic of the pressure driven membrane testing rig

3. Results and discussion

3.1 Materials Characterisation

The TGA results in Fig. 2 indicate that there are no significant variations between the RG samples prepared using different vacuum time. For all the resin gel samples, it is observed that there are four decomposition steps of the gels, which is in line with reports elsewhere [38, 39]. The first step occurs at temperatures up to 200 °C, and the second step between 250 and 330 °C with mass losses of ~8 and ~13 wt% for each step, respectively. The initial mass loss up to 200 °C is associated with physisorbed water. The second mass loss is assigned to the initial onset of carbonisation and thermal decomposition of phenolic compounds [40, 41]. At this second stage, the mass losses of the RG600 and RG1200 samples are slightly higher than the other RG samples. This suggests that the longer vacuum time assisted the release of some volatile organic compounds. The third stage illustrates a large mass loss of approximately 23 wt% between 320 to 700 °C which predominantly correlates with the majority of chemical decomposition and recombination reactions within the carbonized resin structure. This last fourth stage leads to the formation of carbon matrix. The total

mass loss of all RG samples at 700 °C is calculated to be ~46 wt%, suggesting a high yield of the carbonised product.

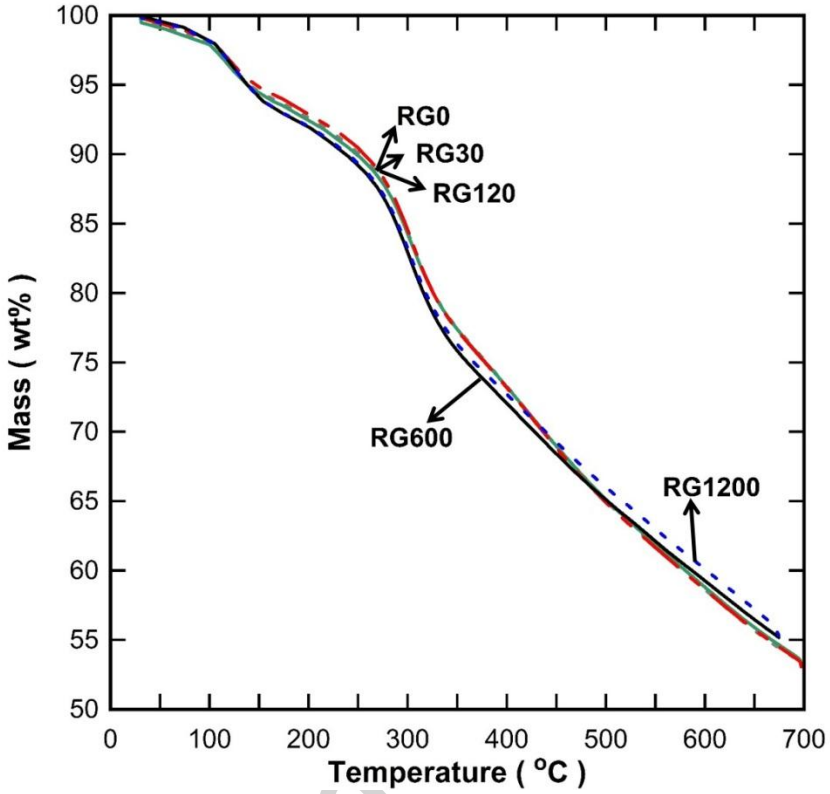

Fig. 2. TGA curves of RG samples exposed to varying vacuum time.

FTIR analysis was carried out to examine the chemical evolution of phenolic resin before and after carbonisation at 700 °C with different applied vacuum times as displayed in Fig. 3. Overall, the FTIR spectra of the dried resin gel samples in Fig. 3a display a large number of peaks overlapping in the lower wavenumbers between 750 and 1750 cm^{-1}, similar to those reported by Roczniak and co-workers [42]. These clusters of peaks in the region from 1700 to 600 cm^{-1} show strong signature bands assigned to hydrocarbons [43]. The strong bands in this region include the C=C stretch of phenyl rings (1600-1500 cm^{-1}), C-H at 1500-1300 cm^{-1}, the broad peak of C-O stretching of phenol (1300-1000 cm^{-1}) and several other smaller peaks related to the C-H stretching bands [44]. Fig. 3a also reveals that the peaks of C-H stretching vibration (2800-3200 cm^{-1}) and C-O stretching (1030

cm^{-1}) are becoming more pronounced as a function of increasing vacuum time. This strongly suggests that the use of vacuum further assisted in the polycondensation of phenol oligomers, which resulted in resin crosslinking [45-47]. This vacuum-assisted reaction is most likely due to the faster drying rates, which leads to increased resin concentration.

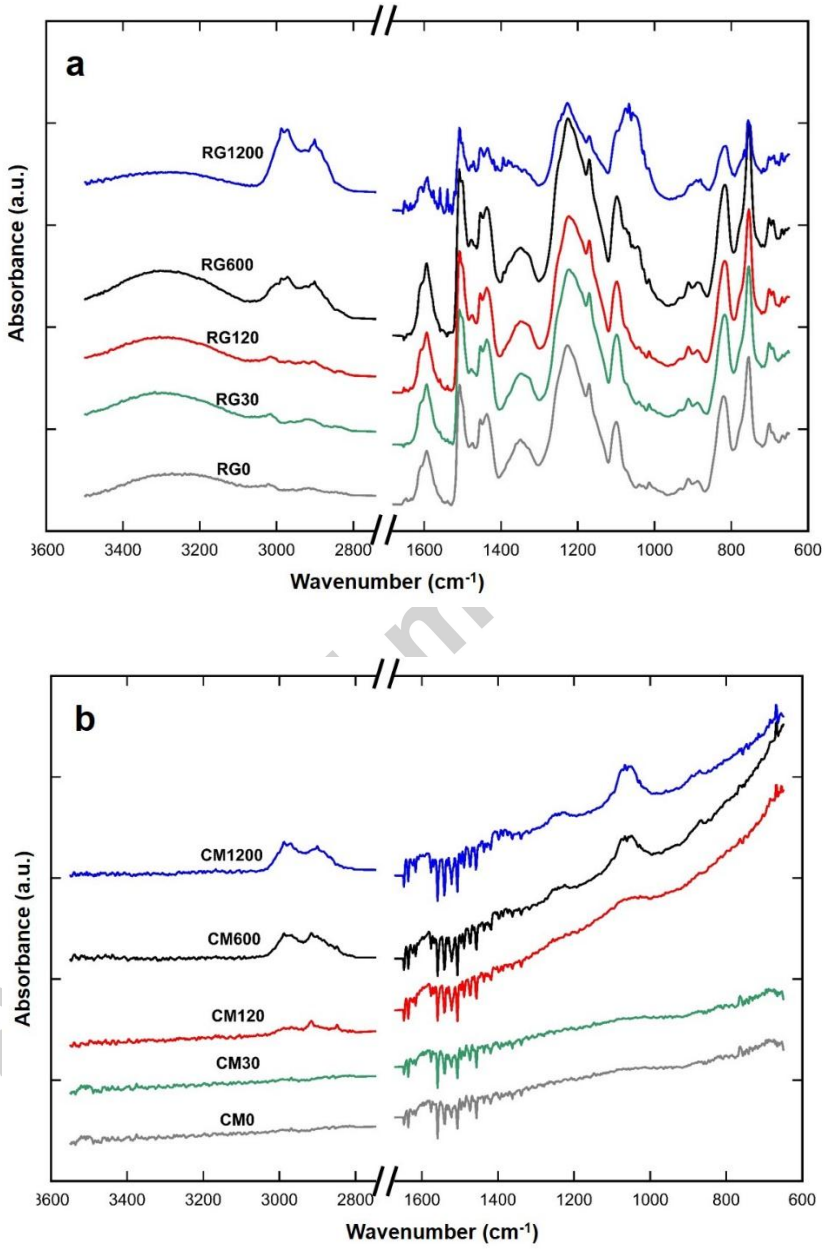

Fig. 3. FTIR spectra of RG and CM materials (a) before and (b) after carbonisation

The FTIR spectra of the CM materials that were carbonised at 700 °C (Fig. 3b) suggest a substantial change has occurred during the carbonisation process. From this figure, most of the strong vibrational peaks characteristics of the hydrocarbons in the fingerprint region (lower wavenumbers) have almost disappeared indicating that these organic functional groups have undergone thermal combustion and carbonization. Interestingly after carbonization, the only remaining groups to be observed in the FTIR are the C-H (2800-3200 cm^{-1}) and C–O (1000-1150 cm^{-1}) peaks, both of which become well-defined and increase in intensity as a function of increasing vacuum time, especially for the CM600 and CM1200 samples. These peaks are attributed to the methylene and ether linkages from the crosslinking reactions which seemed to be preserved even after carbonization treatment.

Nitrogen sorption isotherms for the CM materials are shown in Fig. 4a, which exhibit the combination of typical IUPAC Type-I and Type-VI adsorption/desorption behaviours. This is characteristic of microporous and mesoporous structures, respectively. At very low relative pressures ($p/p_o < 0.01$), the nitrogen isotherms revealed a microporous structure (Type-I) and gradually increase at higher relative pressure (Type-VI) which is attribute to the presence of mesoporous structures. The hysteresis in the desorption branch is almost unnoticeable, but becomes more evident as the vacuum time increases and does indicate an increase in pore size accompanied by a broader pore size distribution. It is interesting to note that the micropore adsorption at very low partial pressures ($p/p_o < 0.01$) are very similar for all the CM samples, but the adsorption increases at higher relative pressure. Table 2 shows that the total pore volume significantly increased by almost three-fold from 0.81 to 2.25 $cm^3\ g^{-1}$ as the vacuum time increased from CM0 to CM1200 samples, respectively.

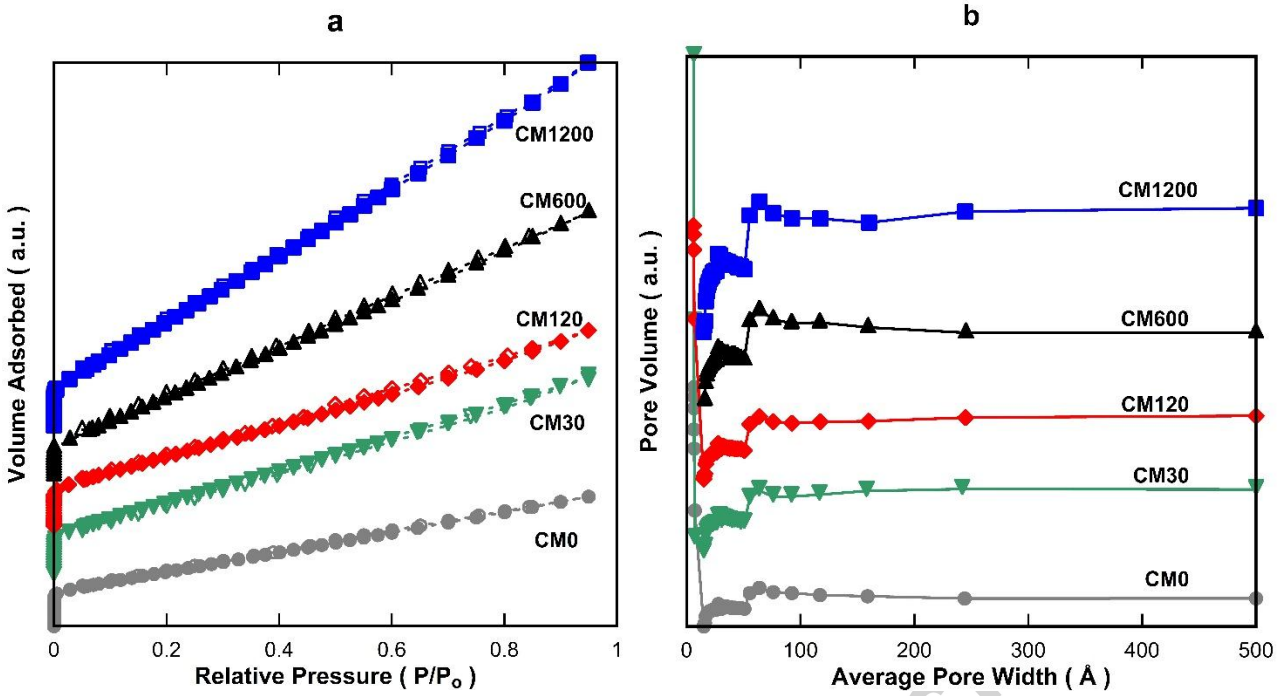

Fig. 4: (a) Nitrogen sorption isotherms and (b) pore size distribution of CM materials.

Table 2 also lists the surface areas of the CM materials. The BET surface area increased significantly as a function of the vacuum time, from 834.5 (CM0) to 1910.5 (CM1200) $m^2\ g^{-1}$, and likewise the total pore volumes from 0.81 (CM0) to 2.25 (CM1200) $cm^3\ g^{-1}$. These results strongly suggest that the exposure to vacuum time conferred the CM matrix with a higher proportion of microporous structure, as the BET surface area is measured at the microporous region of the isotherm at low relative pressures ($p/p_o < 0.20$). Fig. 4b displays the pore size distribution (PSD) based on the Barrett-Joyner-Halenda (BJH) method by using the desorption branch of the isotherms in Fig. 4a. The PSD results clearly indicate the formation of a tri-modal distribution. The first distribution is very narrow and well-defined microporous region below 15 Å. The second distribution starts in the microporous region of 15 Å and broadly extends to mesoporous region of up to 50 Å. The third region is mesoporous starting at 50 Å all the way through to the macroporous region (> 500 Å). Further, increasing the vacuum exposure time led to a systematic increase in both mesoporous and macroporous distributions.

Table 2 – BET surface areas and pore volumes of CM materials.

CM Material	BET Surface Area ($m^2 g^{-1}$)	Microporous Volume ($cm^3 g^{-1}$)	Mesoporous Volume ($cm^3 g^{-1}$)	Macroporous Volume ($cm^3 g^{-1}$)	Total Pore Volume ($cm^3 g^{-1}$)
CM0	834.5	0.31	0.49	0.02	0.81
CM30	1138.6	0.39	0.82	0.03	1.24
CM120	1112.6	0.38	0.81	0.03	1.22
CM600	1436.8	0.39	1.20	0.04	1.64
CM1200	1910.5	0.52	1.66	0.06	2.25

3.2 Membrane characterisation and testing

SEM images of a blank alumina tubular support and the five carbon membranes from no vacuum (CM0) to 1200 seconds (CM1200) of applied vacuum time are shown in Fig. 5. The surface SEM image (Fig. 5a) for the alumina support shows inter-particle voids between alumina particles, contrary to the all CM membranes which show various degree of surface coverage as the voids are mostly plugged by the carbon materials. There are no major differences of surface coverage for all CM membranes (Figs. 5b to 5f). The alumina particle shapes are visible on the surface, contrary to CM thin films which generally cover porous substrates (see schematics in Appendix Fig. A2). This clearly indicates that the phenolic resin covered the alumina particles and also penetrated into the substrate for all the membranes. This is confirmed by the representative cross section of CM0 (Fig. 5g) and CM1200 (Fig. 5h) membranes shows that the phenolic resin penetrated into the alumina substrate between 4.5 and 9.5 µm. This observed penetration effect is closely associated with the contact between a dry porous surface (alumina substrate) and liquid (phenolic resin sol), which induces wetting forces and infiltration of liquid into porous materials [48]. It is also associated with the quality of the substrate, as in this work we did not add interlayers to the alumina substrate, aiming at reducing the production costs of CM membranes. However, the CM1200 membrane thickness is more than twofold higher than the CM0 membrane (i.e. no vacuum). These results suggest that upon the formation of the resin film like the CM0 membrane, the vacuum has then

drawn the phenolic polymers further into the porous substrate. Song and co-workers [22] also reported impregnation of porous substrates by a wet vacuum-assisted method, though their work lead to deep impregnation as phenolic resin sols permeated through the porous alumina support. In this work, a dry vacuum-assisted method was applied once resin thin films were formed, with a minor degree of resin impregnation into the porous substrate. In general, all the membranes do not seem to form a homogenous carbon layer structure.

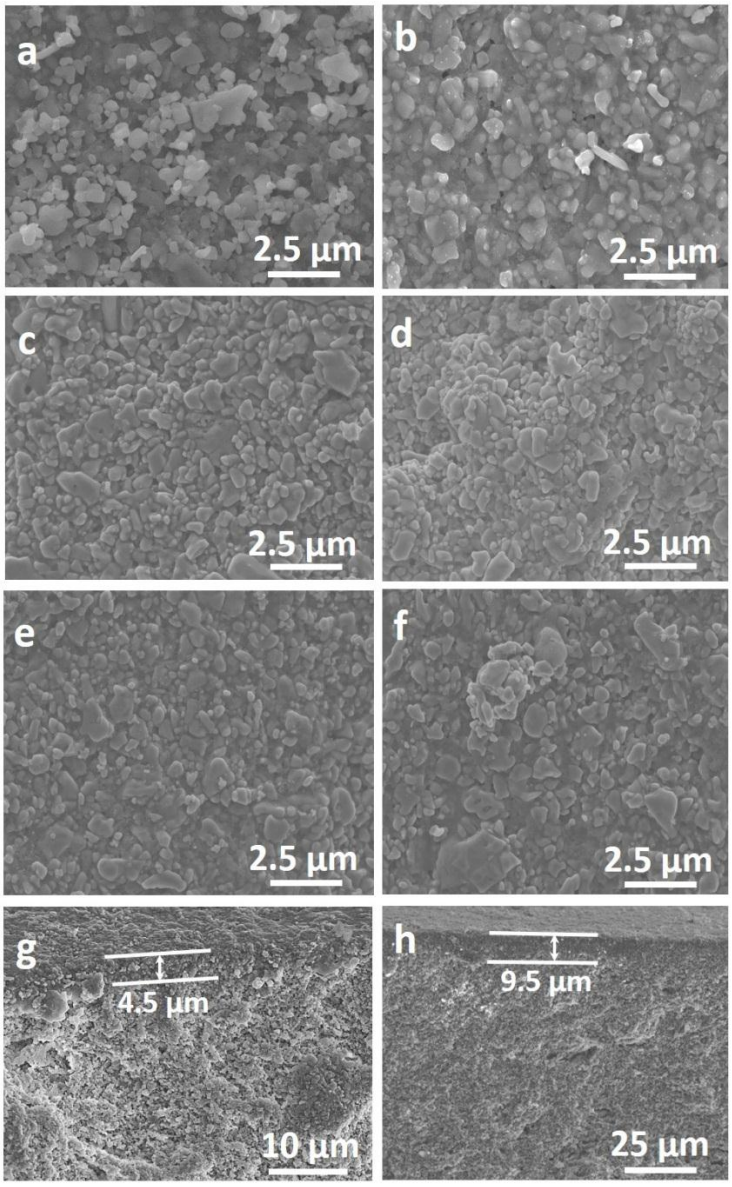

Fig. 5. SEM image of surfaces of (a) an alumina support; membranes (b) CM0, (c) CM30, (d) CM120, (e) CM600 and (f) CM1200; cross sections of (g) CM0 and (h) CM1200.

Fig. 6 shows the water flux permeation for pure water as the feed solution. There is a clear trend observed that water flux permeation of the CM membranes increased gradually with higher pressure and higher vacuum time. Firstly, by increasing the feed pressure, water flux increases due to an increase of the pressure gradient (i.e. driving force) across the membrane. The highest fluxes were measured at 185 and 169 kg m^{-2} h^{-1} at 5 bar for the alumina substrate and CM1200 membrane, respectively. At the equivalent pressure of 5 bar, CM0 (i.e. no vacuum) membrane has the lowest flux with 3.9 kg m^{-2} h^{-1}. At the other end of the pressure gradient (2 bar), CM1200 delivered a water flux of 77 kg m^{-2} h^{-1} but CM0 has only 3.3 kg m^{-2} h^{-1}.

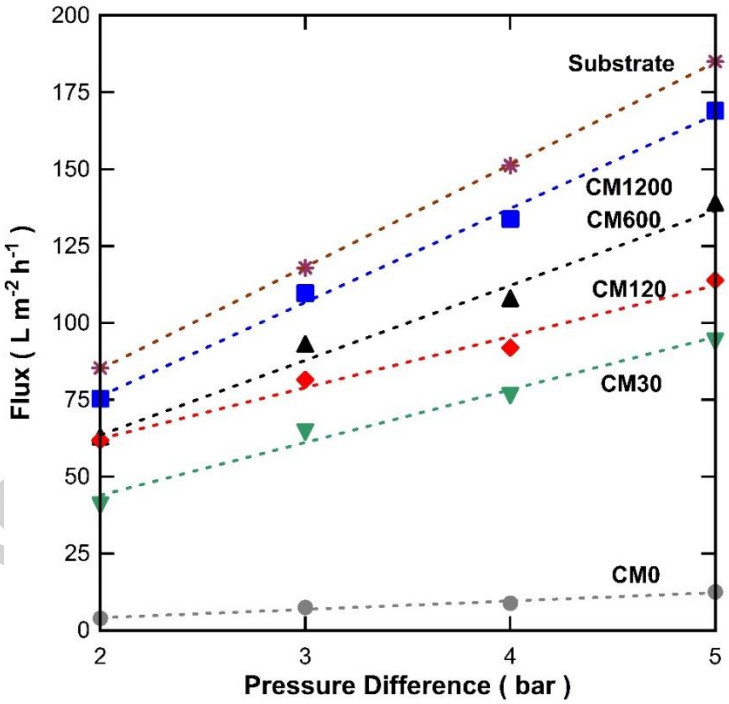

Fig. 6. Water flux (± 7%) at steady state for CM membranes and alumina substrate at 25 C.

The water flux and rejection of molecular weight (MW) cut-off results for water (18 g mol^{-1}), glucose (180 g mol^{-1}), sucrose (342 g mol^{-1}), and PVP (36k and 400k g mol^{-1}) are displayed in Figs. 7a and 7b. The first trend observed confirms the water flux trends in Fig. 6. As the membranes are exposed to longer vacuum times, higher water fluxes are observed in in all the different organic substances. A second trend is that the water fluxes generally decreased as the MW of the organics increased, though there are a few minor variations. The CM0 membrane was non-permeable to the majority of the substances, except for water and glucose. The CM30 membrane was permeable to all MW cut-off solutions, thus showing the onset of pore opening by the vacuum-assisted method. However, the water fluxes reduced abruptly by almost threefold from pure water to glucose solution, and then slightly reduced as the MW increased to sucrose, PVP36k and PVP400k. The membranes exposed to higher vacuum times (CM120, CM600 and CM1200) gave a different trend as the fluxes for pure water and glucose solution were quite similar (CM120 and CM600) or changed slightly only (CM1200). However, the slightly increase in MW from glucose to sucrose resulted in an abrupt reduction in flux. These results clearly indicate that the vacuum-assisted method has an effect in tailoring the pore size structure of the CM membranes.

Further evidence of the vacuum effect on structural tailoring is provided by plotting the rejection results versus the MW as displayed in Fig. 7b. The CM0 rejected (100%) all the organic substances tested except water. As the kinetic diameter of water is 0.26 nm and the diameters of sucrose and glucose are 0.86 nm [49] and 0.9 nm [50], these results strongly suggest that the CM0 membranes have pores well below 0.86 nm. All membranes exposed to vacuum could not reject glucose and sucrose, thus giving a clear indication that pore sizes of CM30 to CM1200 membranes have increased well above 0.9 nm. Nevertheless, a rejection of 80% was observed for PVP36k for the CM30, and 35-45% for the other membranes. Finally, all CM membranes fully rejected the higher MW of PVP400k. These results are interesting as all membranes are characterised by a very broad pore size distribution as shown in Fig. 4b. The ability of the CM0 membrane to reject even glucose strongly suggests that the membrane has percolation pathways containing micro/meso/macro pores (see Table 2), though rejection is controlled by the micropores. This means that the larger mesopores and macropores are linked within the micropores of the CM0 matrix. In the case of the membranes exposed to vacuum, the MW cut-off results suggest that the percolation pathways changed, with a clear indication that microporosity is no longer the controlling mechanism for

rejection. Table 2 shows that under vacuum the mesoporous regions increased significantly whilst the contribution of the macropore region is very marginal and could be neglected. Therefore, the effect of vacuum in crosslinking the phenolic resin as ascertained by FTIR analysis (Fig. 3b), coupled with the results of water fluxes (Fig. 6) and MW cut-off (Fig. 7), indicate that the percolation pathways were modified, leading to the formation of new pathways controlled by the mesopores ($2 \leq d_p \leq 50$ nm).

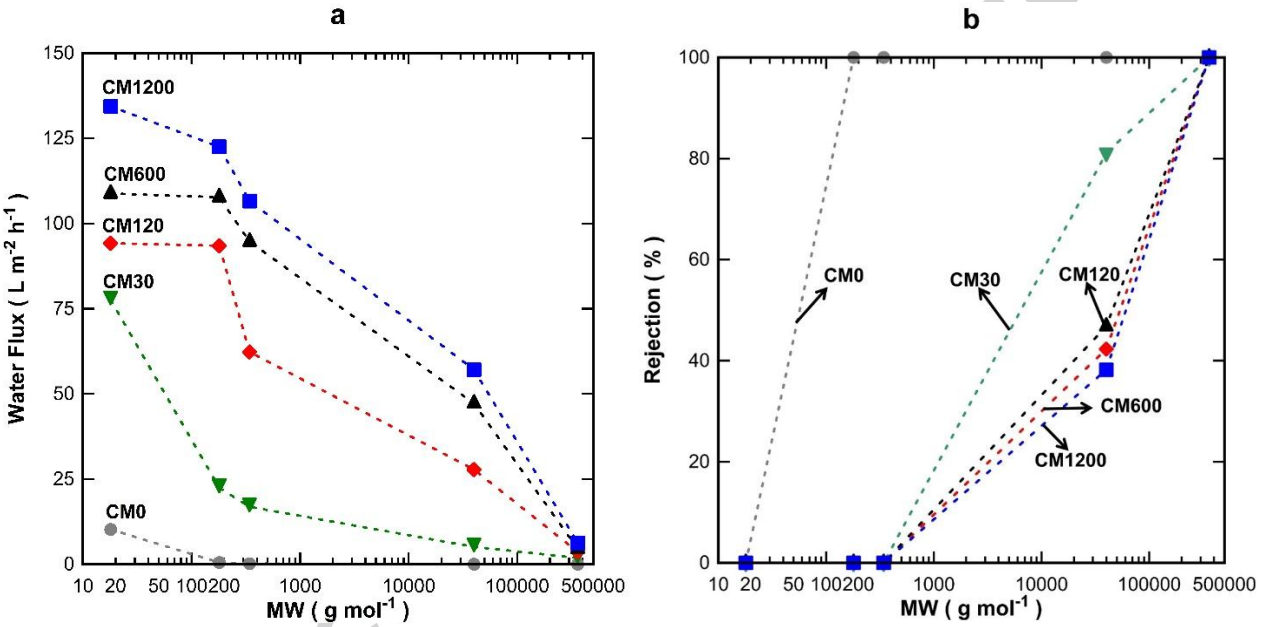

Fig. 7. (a) Water flux and (b) organic rejection of CM membranes.

3.3 Structural tailoring by vacuum

The water flux and rejection results of the CM membranes coupled with the morphological features of the CM materials exposed to varying vacuum times are interesting and warrant further discussions on the potential mechanism of structural formation. It is proposed that the morphological features of the CM material are due to the effect of vacuum leading to a cluster to

cluster aggregation of phenolic resin in a sequential manner as schematically depicted in Fig. 8 and described as follows:

1) By applying vacuum, the longer the vacuum time the more likely that the functional groups of the phenolic resin would be brought into closer proximity for the crosslinking reaction.

2) Crosslinking reaction caused by the clustering of polymeric chains increases microporosity and surface area.

3) As cluster to cluster formation proceeded as a function of the vacuum time, the gap between the clusters, or the inter-cluster space, increased and that caused an increase in total pore volume, accompanied by a broadening of the pore size distribution.

The crosslinking of functional groups, as ascertained by the FTIR spectra (Fig. 3a), shows that the characteristic vibrational stretchings for C=C, C–C, C–H, OH, C–OH groups of the precarbonized resin greatly diminished after carbonization (Fig. 3b). Also, it is observed that a greater peak intensity around 2800–3200 cm^{-1} for the CH_2 linking group and 1030 cm^{-1} for the C–O ether linking group occurred on the expense of the OH stretching peak broadly around 3300 cm^{-1}.

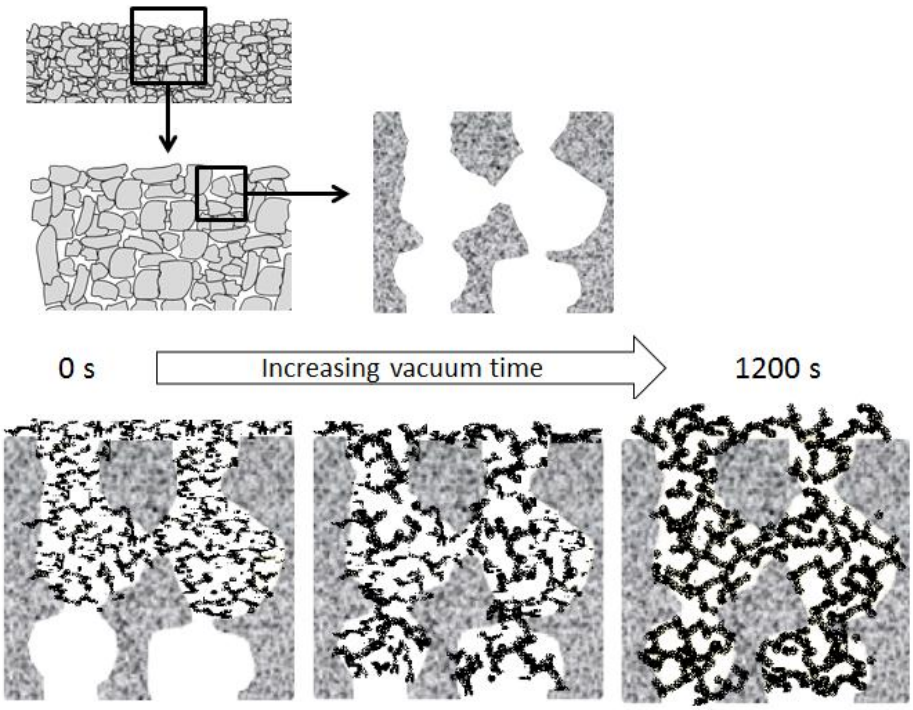

Fig. 8. Schematic of the effect of the vacuum exposure time on the cluster to cluster mechanim of formation of CM materials and membranes.

A final proof of the proposed cluster to cluster aggregation mechanism is supported by the performance of the membranes. The lowest water flux was measured for the CM0 membrane, which increased sequentially as a function of the vacuum exposure time in the order of CM0<CM30<CM120<CM600<CM1200. The highest water flux was reached by the CM1200 of 169 kg m^{-2} h^{-1} at 5 bar, which was 91% higher than the CM0 membrane. The CM membrane performance results correlated very well with the CM membrane morphological features. It is well known that materials with higher total pore volumes and surface area deliver higher fluxes as clearly indicated in Fig. 4 and Table 2.

Nitrogen adsorption analysis revealed that the CM materials resulted in a tri-model pore size distribution (Fig. 4b). It was also observed that the vacuum time exposure played an important role in tailoring the structure of the CM materials, as increasing the vacuum time led to a significant increase in the total pore volume and BET surface area. As the latter is generally calculated for the

first nitrogen adsorbed layer, and that microporous structures have higher surface area than mesoporous structures, these results clearly indicate that increasing the vacuum time conferred a higher degree of microporosity, particularly that the surface area of CM1200 was measured very high reaching values close to 2000 m^2 g^{-1}.

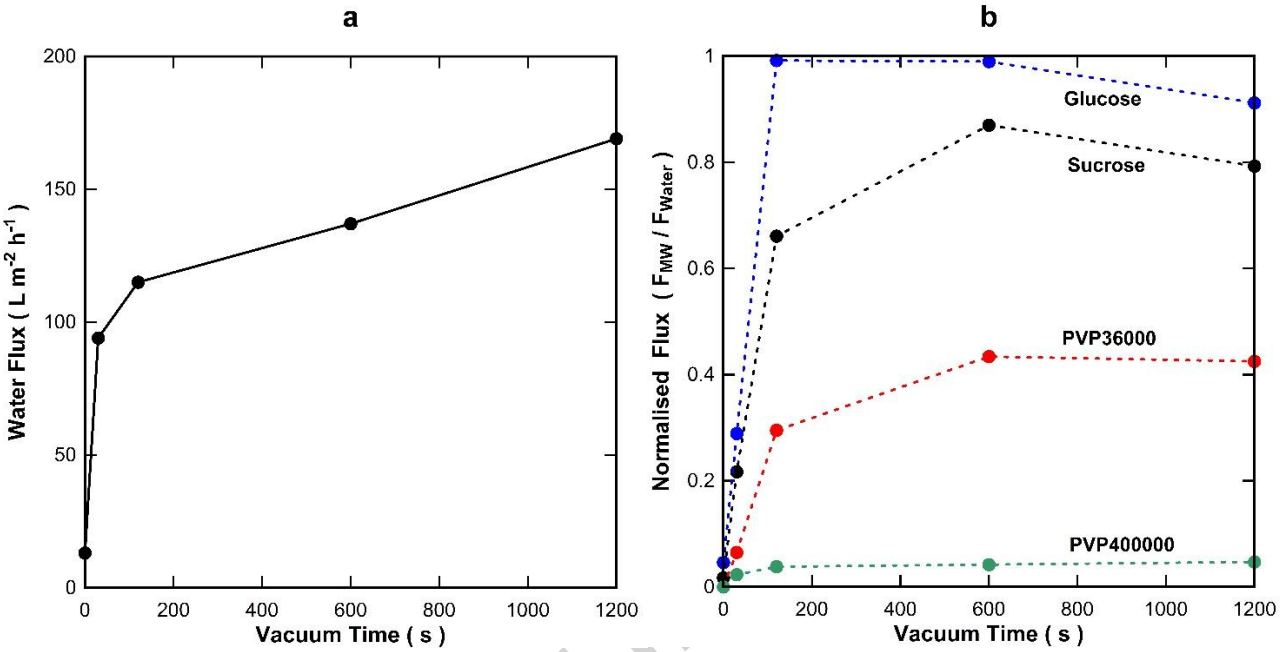

Fig. 9. (a) Water flux (± 7%) of membranes at 5 bar and (b) normalised flux as a function of the membrane vacuum exposure time.

In order to further understand the vacuum effect in tailoring the structure of the CM membranes, Fig. 9b provides an indication of the normalised flux calculated from the flux of the MW cut-off solution divided by the pure water flux for each membrane. Since a water molecule has a kinetic diameter of 0.26 nm, the reduction in the normalised flux signifies that membrane pores were blocked due to the presence of the organics with larger molecular size. The normalized flux of CM0 membrane was determined to be 0.04 and 0.02 for glucose and sucrose solutions which means the membrane was able to block these organics up to 96 and 98%, respectively. In another word, only 4 and 2% of the porous structures were accessible to water permeation only. In fact, CM0 was prepared using a conventional method of carbon molecular sieve membranes tailored for gas

separation, where average pores are generally between 2.5 to 5.0 nm. Hence, this explain the extremely low fluxes observed by the CM0 membranes. The MW cut-off results for the CM30 membrane strongly suggest that ~71% of the porosity was blocked by the glucose, which increased to ~78% by the sucrose, followed by ~93% to ~97% by the PVP36k and PVP400k molecules, respectively. The membranes prepared with high vacuum times (CM120, CM600 and CM1200) present relatively lower pore obstructions for all the organic substances tested, clearly indicating that the pore size broadening of the CM membranes becomes more prevalent for vacuum time in excess of 30 s.

4. Conclusions

This work shows that vacuum played a major role in structural tailoring of carbon membranes. Water fluxes increased as a function of the vacuum time, which correlated well with pore volume and BET surface area increased. The nitrogen isotherms clearly showed the formation of a microporous region and other mesoporous and macroporous regions. MW cut-off tests showed the fluxes the carbon membranes could not reject the smaller molecules of glucose and sucrose, though high rejections of 80% and 100% were achieved from PVP polymers with 36kD and 400kD. Further characterisation clearly indicates that reactions of the phenolic resin occurred since the onset of the vacuum exposure, and the cross-linking of phenolic oligomers increases as a function of the vacuum time. The characterisation results, coupled with the membrane results, strongly suggest a cluster-to-cluster mechanism, leading to the aggregation of the phenolic compounds in close proximity, thus forming microporosity within the clusters, and meso and macroporosity between the clusters.

Acknowledgement

S.N. Abd Jalil gratefully acknowledges the generous financial scholarship support from Ministry of Higher Education Malaysia (MOHE) and Universiti Teknologi MARA (UiTM). D.K. Wang thanks the awards given by the ARC Discovery Early Career Researcher Award (DE150101687) and the

American Australian Association Chevron Fellowship. J. C. Diniz da Costa acknowledges support given by the Australian Research Council (ARC) Future Fellowship program (FT130100405).

Appendix

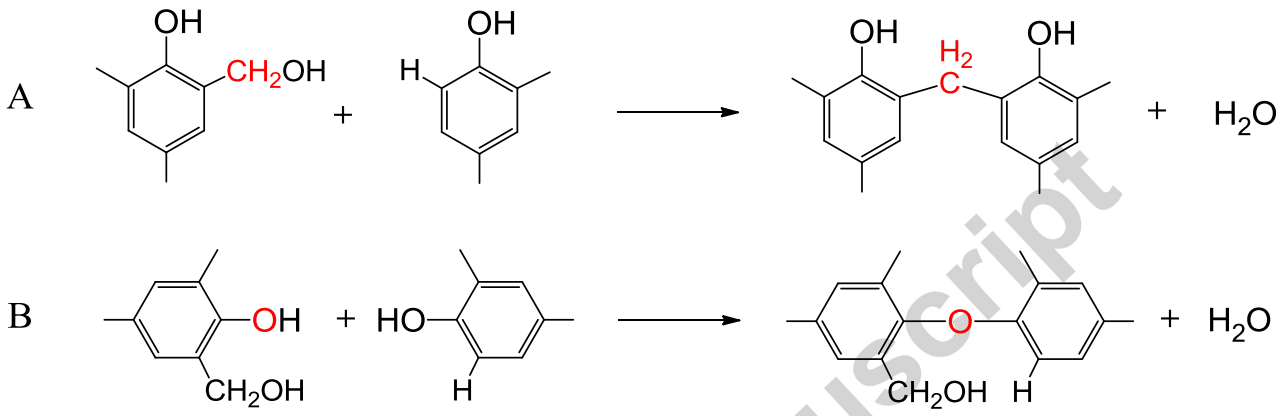

Fig. A1. Condensation of phenolic resin leading to the formation of (A) CH_2 methylene and (B) C–O ether linkages.

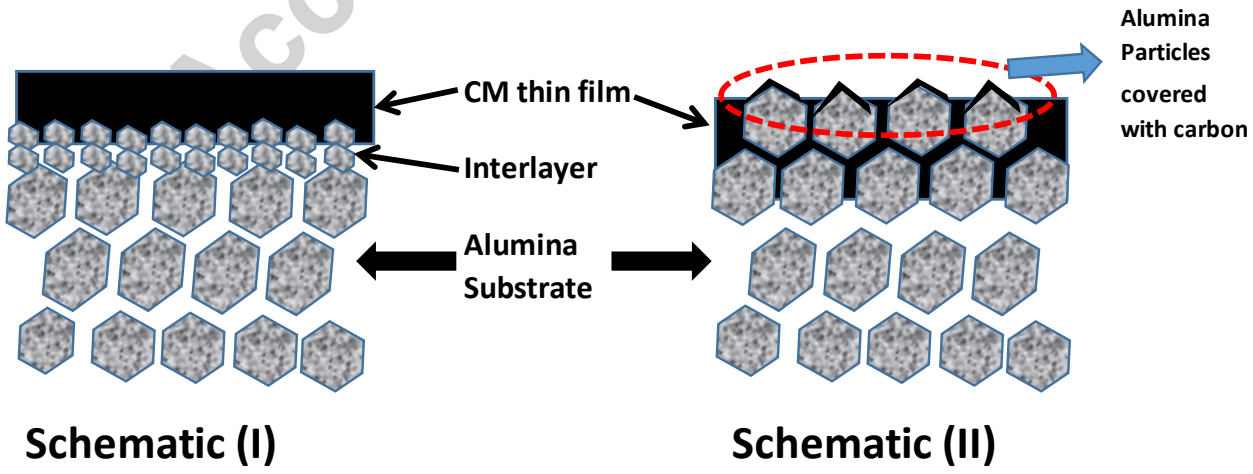

Fig. A2. Schematics of (I) conventional CMS membranes prepared on alumina substrates with interlayers and (II) this work.

References

[1] L. Dahdouh, M. Delalonde, J. Ricci, A. Servent, M. Dornier, C. Wisniewski, Size-cartography of orange juices foulant particles: Contribution to a better control of fouling during microfiltration, J. Membr. Sci. 509 (2016) 164-172.

[2] X.B. Ke, R.F. Shao, H. Zhu, Y. Yuan, D.J. Yang, K.R. Ratinac, X.P. Gao, Ceramic membranes for separation of proteins and DNA through in situ growth of aluminananofibres inside porous substrates, Chem. Commun. 10 (2009) 1264-1266.

[3] E.N. Tummons, V.V. Tarabara, J.W. Chew, A.G. Fane, Behavior of oil droplets at the membrane surface during crossflow microfiltration of oil–water emulsions, J. Membr. Sci. 500 (2016) 211-224.

[4] X. Zhang, D.K. Wang, D.R. Schmeda Lopez, J.C. Diniz da Costa, Nanostructured anti-fouling TiO_2 hollow fiber membrane for water purification, Chem. Eng. J. 236 (2014) 314–322.

[5] C. Yang, G. Zhang, N. Xu, J. Shi Preparation and application in oil–water separation of ZrO_2/α-Al_2O_3 MF membrane, J. Membr. Sci. 142 (1998) 235-243.

[6] W. Doyen, W. Adriansens, B. Molenberghs, R. Leysen, A comparison between polysulfone, zirconia and organo-mineral membranes for use in ultrafiltration, J. Membr. Sci. 113 (1996) 247-258.

[7] M. Kondo, H. Kita, Permeation mechanism through zeolite NaA and T-type membranes for practical dehydration of organic solvents, J. Membr. Sci. 361 (2010) 223-231.

[8] X. Yang, L. Ding, M. Wolf, F. Velterop, H.J.M. Bouwmeester, S. Smart, J.C. Diniz da Costa, A. Liubinas, J.-D. Li, J. Zhang, M. Duke, Pervaporation of ammonia solution with γ-alumina supported organosilica membranes, Sep. Purif. Technol. 168 (2016) 141–151.

[9] M. Elma, D.K. Wang, C. Yacou, J.C. Diniz da Costa, Interlayer-free P123 carbonised template silica membranes for desalination with reduced salt concentration polarisation, J. Membr. Sci. 475 (2015) 376–383

[10] J. Koresh, A. Sofer, Molecular sieve carbon permselective membrane. Part I. Presentation of a new device for gas mixture separation, Sep. Sci. Technol. 18 (1983) 723-734.

[11] V. C. Geiszler, W. J. Koros, Effects of polyimide pyrolysis conditions on carbon molecular sieve membrane properties. Ind. Eng. Chem. Res. 35 (1996) 2999-3003.

[12] Y. Kusuki, H. Shimazaki, N. Tanihara, S. Nakanishi, T. Yoshinaga, Gas permeation properties and characterization of asymmetric carbon membranes prepared by pyrolyzing asymmetric polyimide hollow fiber membrane, J. Membr. Sci. 134 (1997) 245-253.

[13] K. Wang, H. Suda, K. Haraya, The characterization of CO_2 permeation in a CMSM derived from polyimide, Sep. Purif. Technol. 31 (2003) 61-69.

[14] H. Wang, L. Zhang, G.R. Gavalas, Preparation of supported carbon membranes from furfuryl alcohol by vapor deposition polymerization, J. Membr. Sci. 177 (2000) 25-31.

[15] G.T. Qin, C. Wang, W. Wei, Preparation of a mesoporous carbon membrane from resorcinol and formaldehyde, Carbon 48 (2010) 4206-4208.

[16] W. Wei, H.Q. Hu, L.B. You, G.H. Chen, Preparation of carbon molecular sieve membrane from phenol-formaldehyde Novolac resin, Carbon 40 (2002) 465-467.

[17] T.A. Centeno, A.B. Fuertes, Carbon molecular sieve membranes derived from a phenolic resin supported on porous ceramic tubes, Sep. Purif. Technol. 25 (2001) 379-384.

[18] W. Wei, G.T. Qin, H.Q. Hu, L.B. You, G.H. Chen, Preparation of supported carbon molecular sieve membrane from novolac phenol-formaldehyde resin, J. Membr. Sci. 303 (2007) 80-85.

[19] V.M. Linkov, R.D. Sanderson, E.P. Jacobs, Highly asymmetrical carbon membranes, J. Membr. Sci. 95 (1994) 93-99.

[20] X. Ma, R. Swaidan, B. Teng, H. Tan, O. Salinas, E. Litwiller, Y. Han, I. Pinnau, Carbon molecular sieve gas separation membranes based on an intrinsically microporous polyimide precursor, Carbon 62 (2013) 88–96.

[21] C. Song, T. Wang, Y. Pan, J. Qiu, Preparation of coal-based microfiltration carbon membrane and application in oily wastewater treatment, Sep. Purif. Technol. 51 (2006) 80-84.

[22] Y. Song, D.K. Wang, G. Birkett, W. Martens, S. Smart, J.C. Diniz da Costa, Mixed matrix carbon molecular sieve and alumina (CMS-Al_2O_3) membranes, Scient. Rep. 6 (2016) 30703 DOI: 10.1038/srep3070.

[23] A. Sakoda, T. Nomura, M. Suzuki, Activated carbon membrane for water treatments: Application to decolorization of coke furnace wastewater, Adsorption, 3 (1997) 93-98.

[24] Y. Sakata, A. Muto, Md.A. Uddin, H. Suga, Preparation of porous carbon membrane plates for pervaporation separation applications, Sep. Purif. Technol. 17 (1999) 97–10.

[25] C. Li, C. Song, P. Tao, M. Sun, Z. Pan, T. Wang, M. Shao, Enhanced separation performance of coal-based carbon membranes coupled with an electric field for oily wastewater treatment, Sep. Purif. Technol. 168 (2016) 47-56

[26] G. Pugazhenthi, S. Sachan, N. Kishore, A. Kumar, Separation of chromium (VI) using modified ultrafiltration charged carbon membrane and its mathematical modelling, J. Membr. Sci. 254 (2005) 229-239.

[27] Y. Pan, W. Wang, T. Wang, P. Yao, Fabrication of carbon membrane and microfiltration of oil-in-water emulsion: An investigation on fouling mechanisms, Sep. Purif. Technol. 57 (2007) 388-393.

[28] M.A. Llosa Tanco, D.A. Pacheco Tanaka, A. Mendes, Composite-alumina-carbon molecular sieve membranes prepared from novolac resin and boehmite. Part II: Effect of the carbonization temperature on the gas permeation properties, Int. J. Hydrogen Energy 40 (2014) 3485–3496.

[29] C.J. Anderson, S.J. Pas, G. Arora, S.E. Kentish, A.J. Hill, S.I Sandler, G.W. Stevens, Effect of pyrolysis temperature and operating temperature on the performance of nanoporous carbon membranes, J. Membr. Sci. 322 (2008) 19-27.

[30] M.A. Llosa Tanco, D.A. Pacheco Tanaka, S.C. Rodrigues, M. Teixeira, A. Mendes, Composite-alumina-carbon molecular sieve membranes prepared from novolac resin and boehmite. Part I: Preparation, characterization and gas permeation studies, Int. J. Hydrogen Energy 40 (2015) 5653–5663.

[31] M. Teixeira, M.C. Campo, D.A. Pacheco Tanaka, M.A. Llosa Tanco, C. Magen, A. Mendes, Composite phenolic resin-based carbon molecular sieve membranes for gas separation, Carbon 2011, 49, 4348–4358.

[32] M. Teixeira, S. Rodrigues, M.C. Campo, D.A. Pacheco Tanaka, M.A. Llosa Tanco, L. Madeira, J. Sousa, A. Mendes, A. Boehmite-phenolic resin carbon molecular sieve membranes - permeation and adsorption studies, Chem. Eng. Res. Des. 92 (2014) 2668-2680.

[33] M. Teixeira, M.C. Campo, D.A. Pacheco Tanaka, M.A. Llosa Tanco, C. Magen, A. Mendes, Carbon–Al_2O_3–Ag composite molecular sieve membranes for gas separation, Chem. Eng. Res. Des. 90 (2012) 2338–2345.

[34] T.A. Centeno, A.B. Fuertes, Supported carbon molecular sieve membranes based on a phenolic resin, J. Membr. Sci. 160 (1999) 201-211.

[35] T.A. Centeno, J.L. Vilas, A.B. Fuertes, Effects of phenolic resin pyrolysis conditions on carbon membrane performance for gas separation, J. Membr. Sci. 228 (2004) 45-54.

[36] X. Wang, Q. Zhu, S.M. Mahurin, C. Liang, S. Dai, Preparation of free-standing high quality mesoporous carbon membranes, Carbon 48 (2010) 557-560.

[37] W. Zhou, M. Yoshino, H. Kita, K.I. Okamoto, Preparation and gas permeation properties of carbon molecular sieve membranes based on sulfonated phenolic resin, J. Membr. Sci. 217 (2003) 55-67.

[38] J. Wang, H. Jiang, N. Jiang, Study on the pyrolysis of phenol-formaldehyde (PF) resin and modified PF resin, Thermoch. Acta 496 (2009) 136-14.

[39] Y.J. Kim, M.I. Kim, C.H. Yun, J.Y. Chang, C.R. Park, M. Inagaki, Comparative study of carbon dioxide and nitrogen atmospheric effects on the chemical structure changes during pyrolysis of phenol–formaldehyde spheres, J. Coll. Interface Sci. 274 (2004) 555-562.

[40] Y.K. Kim, H.B. Park, Y.M. Lee, Carbon molecular sieve membranes derived from thermally labile polymer containing blend polymers and their gas separation properties, J. Membr. Sci. 243 (2004) 9-17.

[41] T.A. Centeno, A.B. Fuertes, Carbon molecular sieve gas separation membranes based on poly(vinylidene chloride-co-vinyl chloride), Carbon 38 (2000) 1067-1073.

[42] K. Roczniak, T. Biernacka, M. Skarżyński, Some properties and chemical structure of phenolic resins and their derivatives, J. Appl. Polymer Sci. 28 (1983) 531-542.

[43] G. Socrates, Infrared and Raman characteristic group frequencies: tables and charts (2004), John Wiley & Sons.

[44] K. Ouchi, Infra-red study of structural changes during the pyrolysis of a phenol-formaldehyde resin, Carbon 4 (1966) 59-66.

[45] A. Izumi, T. Nakao, M. Shibayama, Gelation and cross-link inhomogeneity of phenolic resins studied by ^{13}C-NMR spectroscopy and small-angle X-ray scattering, Soft Matter 9 (2013) 4188-4197.

[46] X. Zhang, M.G. Looney, D.H. Solomon, A.K. Whittaker, The chemistry of novolac resins: 3. ^{13}C and ^{15}N n.m.r. studies of curing with hexamethylenetetramine, Polymer 38 (1997) 5835-5848.

[47] L. Costa, L. Rossi di Montelera, G. Camino, E.D. Weil, E.M. Pearce, Structure-charring relationship in phenol-formaldehyde type resins, Polymer Degrad. Stab. 56 (1997) 23-35.

[48] P. Joos, P. Van Remoortere, M. Bracke, The kinetics of wetting in a capillary, J. Coll. Interface Sci. 136 (1990) 189-197.

[49] J. Jae, G.A. Tompsett, A.J. Foster, K.D. Hammond, S.M. Auerbach, R.F. Lobo, G.W. Huber, Investigation into the shape selectivity of zeolite catalysts for biomass conversion, J. Catal. 279 (2011) 257-268.

[50] L.E. Ramm, M.B. Whitlow, M.M. Mayer, Transmembrane channel formation by complement: functional analysis of the number of C5b6, C7, C8, and C9 molecules required for a single channel, Proceed. National Academy Sci. 79 (1982) 4751-4755.

Highlights

- Carbon membranes derived from phenolic resin by a vacuum-assisted method.
- Significant pore volume (2.2 cm^3 g^{-1}) and surface area (1910 m^2 g^{-1}) with vacuum.
- Water flux increased by 91% as vacuum time for membranes was raised from 0 to 1200s.
- Vaccum assisted the polycondensation reactions of phenolic oligomers.
- Vacuum promoted a cluster aggregation mechanism with micro/mesoporous regions.